

Magnetization self-organization in a single-domain ferromagnet subject to a spin current

P. M. Gorley^{1,†}, P. P. Horley¹, V. K. Dugaev², J. Barnaś³, and W. Dobrowolski⁴

¹*Department of Electronics and Energy Engineering,*

Chernivtsi National University, 2 Kotsyubynsky St., 58012 Chernivtsi, Ukraine

²*Department of Physics and CFIF, Instituto Superior Técnico, Av. Rovisco Pais, 1049-001 Lisbon, Portugal, and Frantsevich Institute for Problems of Materials Science, National Academy of Sciences of Ukraine, 5 Vilde St., 58001 Chernivtsi, Ukraine*

³*Department of Physics, Adam Mickiewicz University, Umultowska 85, 61-614 Poznań, and Institute of Molecular Physics, Polish Academy of Sciences,*

M. Smoluchowskiego 17, 60-179 Poznań, Poland

⁴*Institute of Physics, Polish Academy of Sciences, Al. Lotników 32/46, 02668 Warszawa, Poland*
(Dated: May 5, 2019)

The Landau-Lifshitz equation for the magnetization dynamics of a single-domain magnetic system is solved using the methods of self-organization. The description takes into account the torque due to spin transfer. The potential energy of the system includes the uniaxial and easy-plane anisotropies, and the Zeeman energy due to an external magnetic field. The equilibrium and stationary states are investigated as a function of the spin current and external magnetic field. The presented bifurcation diagram allows to determine the margins of a neutral stability mode of the equilibrium and stationary states for different values of the easy-plane anisotropy constant. Using the power spectral density method, the trajectory tracing, Hausdorff dimension, and maximum Lyapunov exponent, the dynamics of the phase states in an external magnetic field is demonstrated. The analytical transcendent equations for switching between different equilibrium states are also obtained, proving the importance of phase averaging.

PACS numbers: 85.75.-d, 72.25.-b, 05.65.+b, 05.45.-a

I. INTRODUCTION

Spintronics is a new and intensively developing field of physics, which attracts significant scientific interest from both fundamental and application points of view (see, e.g., Refs. [1,2,3,4,5,6] and the references therein). The main objective of spintronics is search for new materials for devices of future generation (like, for instance, spin transistors, quantum computing devices, solar cells, etc.) and with fundamentally new operation principles in comparison to traditional devices based on the electron charge transport.^{7–9} One of the main problems, which still require solution, concerns effective control of spin polarization and spin injection in spintronics devices.^{2,3,10–12} This problem triggered an extensive theoretical and experimental search for new materials and devices, like metallic systems consisting of ferromagnetic and nonmagnetic layers or tunnel junctions including ferromagnetic and diluted magnetic (non-magnetic) semiconductors.^{1,4–6} Significant progress has been made recently in the technology and physics of doped semiconductors with spontaneous spin polarization, and in the spin injection from magnetic to non-magnetic systems.^{13–33} Several theoretical models have been also proposed to describe doping-induced ferromagnetism and spin injection.^{13,14,15,16,17,18,19,20}

Theoretical studies carried out to date usually treated the spin subsystem by techniques developed for equilibrium situations. However, such an approach applied to the spin-transport phenomena ignores the fact that

both spin polarization and spin injection are dynamical processes and therefore should be treated by methods of non-equilibrium thermodynamics.^{34–37} This is particularly important for open dynamical systems that are able to exchange particles and energy with the environment (which is true for the spin subsystem considered here). The dynamical processes may lead to stationary non-equilibrium states with high ordering level. Such cooperative phenomena in the system of magnetic ions and mobile band electrons can take place far from an equilibrium state. Generally, the system can have several stationary solutions described by the same set of nonlinear time-dependent differential equations, which are different regarding their stability against small fluctuations.

In the case of stable solution, fluctuations are suppressed within a short period of time. If a solution is unstable, fluctuations can be amplified and the system may be switched to another stable state. The new state may have the same or even higher ordering level, when it is described with a lower symmetry group. Such spontaneous switching between different possible states is known as a self-organization of the system. The methodology based on non-equilibrium thermodynamics, developed for investigating self-organization processes, offers promising approach to such spintronics problems like spin polarization and spin injection. This may lead to new quantitative and even qualitative results, which are not accessible within the traditional approaches.

The problem studied in this paper concerns the dynamics of a single-domain magnetic system interacting with a spin current flowing through it – the problem al-

ready investigated in detail by Sun²⁰ using the standard methods. The approach based on the self-organization techniques yields some new interesting results.

The paper is organized as follows. The model is described in Section 2, where the symmetry of a quasi-one-dimensional ferromagnet²⁰ is analyzed in detail. Analytical solutions corresponding to four equilibrium and two independent stationary states are also derived there. The stability analysis regarding the influence of small perturbations shows that the spatial angles describing the magnetization vector can vary either monotonically or in an oscillatory manner with time, depending in a complex way on the system parameters.

Section 3 presents the results of our numerical calculations and the relevant discussion. This section is split into two subsections in order to separate the analysis of equilibrium and stationary states from the analysis of the time evolution of the system. We also discuss the magnetization switching and its dependence on the magnetic field and spin current. It is shown that the equilibrium and stationary states are characterized by a different dynamics of the oscillatory modes which can be excited by small perturbations of the phase variables. The bifurcation points of the system (the points where the system changes its behavior qualitatively) are also determined, and their dependence on the external parameters is investigated. The second subsection presents the results obtained from the numerical simulations. A significant attention is paid to the analysis of the system evolution through several types of different magnetization precession modes. It is shown that the system can be switched between different equilibrium states, $m_z = \pm 1$, in a controllable way, which is of particular interest for the spintronics applications. The detailed analysis of the system evolution has been performed using the self-organization methodology; namely, the density histogram of the longitudinal magnetization component, power spectral density, Hausdorff dimension, maximum Lyapunov exponent, and the phase trajectory tracing curve. This allowed us to clarify peculiarities of the magnetization orientation for different values of the applied magnetic field. The derived analytical expressions for the magnetic switching between the states $m_z = \pm 1$ made it possible to analyze the dependence of the switching time on the external magnetic field and the spin current. The last Section 4 includes the summary and main conclusions.

II. THEORETICAL MODEL AND METHOD

We consider a model system studied recently by Sun.²⁰ Accordingly, we assume a single-domain quasi-one-dimensional ferromagnet of length l_m along the axis x and a square cross-section ($a \times a$) in the plane $y-z$. The system is described by the easy-axis (along the axis z) and easy-plane ($y-z$) magnetic anisotropies. In addition, an external magnetic field \mathbf{H} is applied in the plane $y-z$

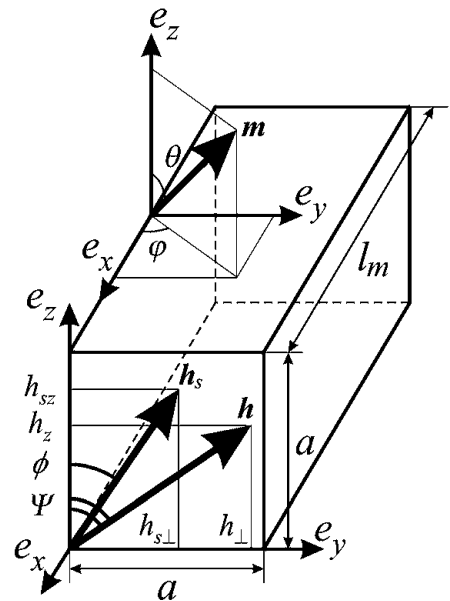


FIG. 1: Model geometry and main variables of the system.

at an angle ψ with respect to the axis z . The external field \mathbf{H} and the easy-plane anisotropy are described in dimensionless relative units, $\mathbf{h} = \mathbf{H}/H_k$ and $h_p = K_p/K$, where $H_k = 2K/M$, K and K_p are respectively the easy-axis and easy-plane anisotropy constants, and M is the absolute value of magnetization.

The system interacts with a spin current \mathbf{J}_s flowing along the wire. The incident spin current is described by the two parameters, η and \mathbf{n}_s . The parameter η describes the degree of spin polarization of the incoming charge current I , whereas \mathbf{n}_s is a unit vector along the corresponding spin polarization. We assume that \mathbf{n}_s is in the $y-z$ plane, and forms an angle ϕ with the axis z . As in Ref. [20], the spin current is described in dimensionless units as $\mathbf{h}_s = \mathbf{n}_s \hbar \eta I / 4e l_m a^2 K$. In the following we restrict considerations to homogeneous dynamics, and assume that the system absorbs the perpendicular to the magnetization component of the incident spin current. This produces an additional torque acting on the system magnetization. The geometry of the system, together with the reference frame used in the theoretical description, are shown in Fig. 1.

As in Ref. [20], we assume that the energy density U includes the energy of uniaxial magnetic anisotropy, $U_K = K \sin^2 \theta$, the energy of easy-plane anisotropy, $U_p = K_p (\sin^2 \theta \cos^2 \varphi - 1)$, and the Zeeman energy due to an external magnetic field, $U_H = -K (h_{\perp} \sin \theta \sin \varphi + h_z \cos \theta)$, where $h_{\perp} = h \sin \psi$ and $h_z = h \cos \psi$ are the components of the vector \mathbf{h} (see Fig. 1). Thus, one can write

$$U_0(\theta, \varphi) \equiv \frac{U(\theta, \varphi)}{K} = Z(\varphi) \sin^2 \theta - 2(h_z \cos \theta + h_{\perp} \sin \theta \sin \varphi), \quad (1)$$

where

$$Z(\varphi) \equiv (1 + h_p \cos^2 \varphi), \quad (2)$$

and a constant term in Eq. (1) has been omitted.

The homogeneous dynamics of the magnetization \mathbf{M} is determined by the Landau-Lifshitz equations,³⁸ including also the torque due to the spin transfer,²⁰

$$\begin{aligned} \frac{\partial \theta}{\partial \tau} &= -\sin \theta (\alpha A_1 + A_2), \\ \frac{\partial \varphi}{\partial \tau} &= \alpha A_2 - A_1, \end{aligned} \quad (3)$$

with

$$\begin{aligned} A_1 &= Z(\varphi) \cos \theta + h_z - \frac{1}{\sin \theta} (h_{\perp} \cos \theta \sin \varphi + h_{s\perp} \cos \varphi), \\ A_2 &= \frac{1}{2} h_p \sin 2\varphi + \frac{1}{\sin \theta} (h_{\perp} \cos \varphi - h_{s\perp} \cos \theta \sin \varphi). \end{aligned} \quad (4)$$

Here, $h_{\perp} = h \sin \psi$ and $h_z = h \cos \psi$ are the applied field components, $h_{s\perp} = h_s \sin \phi$ and $h_{sz} = h_s \cos \phi$ are the components of spin current (see Fig. 1), whereas $\tau = t/[(1 + \alpha^2)/\gamma H_k]$ denotes the dimensionless time, which depends on the gyromagnetic ratio $\gamma = g\mu_b/\hbar$, the anisotropy field H_k , and the damping coefficient α ($\alpha \ll 1$). When writing down the set of Eqs. (3), we assumed that the magnitude of the magnetization vector is constant, and $g = 2$.

It is rather difficult to obtain analytical solution of Eqs. (3) and (4) in a general case. Therefore, in this paper we consider a particular case, when the external magnetic field \mathbf{h} and the spin current \mathbf{h}_s are along the axis z of the reference system shown in Fig. 1 (similarly to the situation considered in Ref. [20]). Thus, we put $h_{\perp} = 0$, $h_z = h$, $h_{s\perp} = 0$ and $h_{sz} = h_s$. Note that from now on, h and h_s denote the z -components of the magnetic field and spin-current. Accordingly, both h and h_s can take either positive or negative values. Consequently, Eqs. (1) and (3) can be rewritten as

$$U_0(\theta, \varphi) = Z(\varphi) \sin^2 \theta - 2h \cos \theta, \quad (5)$$

and

$$\begin{aligned} \frac{\partial \theta}{\partial \tau} &= -\sin \theta \left\{ \alpha [Z(\varphi) \cos \theta + h] + \frac{h_p}{2} \sin 2\varphi + h_s \right\}, \\ \frac{\partial \varphi}{\partial \tau} &= \alpha \left[\frac{h_p}{2} \sin 2\varphi + h_s \right] - [Z(\varphi) \cos \theta + h]. \end{aligned} \quad (6)$$

Equations (6) present a generalization of Eq. (11) from Ref. [20] to arbitrary values of the angle θ (in Ref. [20] only the case of $|\theta| \ll 1$ was considered).

The system described by Eqs. (6) is invariant with respect to the following substitutions

$$\varphi \rightarrow \pi + \varphi, \quad (7)$$

and

$$\begin{aligned} h &\rightarrow h, \quad h_s \rightarrow -h_s, \\ \theta &\rightarrow \pi - \theta, \\ \varphi &\rightarrow \pi - \varphi. \end{aligned} \quad (8)$$

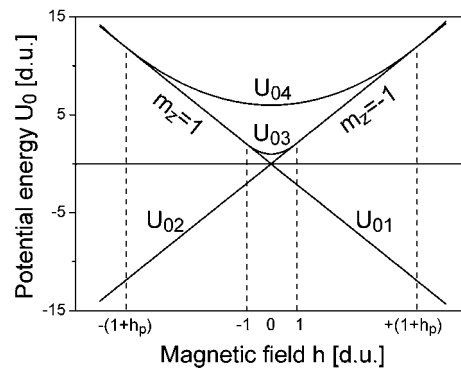


FIG. 2: Possible equilibrium states of the system (here and in the following d.u. means dimensionless units).

The property (7) allows us to reduce the interval of the variable φ to $0 \leq \varphi \leq \pi$, while the relations (8) can be used to verify analytical results, in particular to check the solutions of the characteristic equations.

A. Equilibrium solutions

The equilibrium orientation of the magnetic moment M in the absence of spin current can be found from the conditions³⁹

$$\begin{aligned} \frac{\partial U_0}{\partial \theta} &= 2 \sin \theta_e [Z(\varphi_e) \cos \theta_e + h] = 0, \\ \frac{\partial U_0}{\partial \varphi} &= -h_p \sin^2 \theta_e \sin 2\varphi_e = 0. \end{aligned} \quad (9)$$

From now on we label the equilibrium solutions with the index "e", and the stationary ones with the index "0".

Assuming that $h_p > 0$,²⁰ we find the equilibrium solutions of Eqs. (9)

$$\begin{aligned} (1) \quad & \sin \theta_e = 0, \quad \varphi_e - \text{arbitrary}, \\ (2) \quad & \cos \theta_e = -h, \quad \varphi_e = \pi/2, \\ (3) \quad & \cos \theta_e = -\frac{h}{1+h_p}, \quad \varphi_e = 0. \end{aligned} \quad (10)$$

As follows from Eqs. (10), in the absence of magnetic field, $h = 0$, the system has the following energy states (phases): spin-degenerate states $\mathbf{m} = (0, 0, \pm 1)$ corresponding to the energy $U_0 = 0$, the state $\mathbf{m} = (1, 0, 0)$ with the energy $U_0 = 1$, and the state $\mathbf{m} = (0, 1, 0)$ with the energy $U_0 = 1 + h_p$. Here, \mathbf{m} is the unit vector along the magnetization, $\mathbf{m} = \mathbf{M}/M$. The external magnetic field removes the spin degeneracy, and the level $U_0 = 0$ splits into two sub-levels with the corresponding energies $U_{01} = -2h$ for the state $\mathbf{m} = (0, 0, 1)$ and $U_{02} = 2h$ for the state $\mathbf{m} = (0, 0, -1)$. The magnetic field also leads to precession of the m_z component around the direction of magnetic field for the states $\mathbf{m} = (\sqrt{1-h^2}, 0, -h)$ with energy $U_{03} = 1 + h^2$ and $\mathbf{m} = (0, \sqrt{1-(h/(1+h_p))^2}, -h/(1+h_p))$ with energy

$U_{04} = 1 + h_p + h^2/(1 + h_p)$. The state of energy U_{03} exists in a certain range of magnetic fields, $0 \leq |h| \leq 1$, while the state U_{04} corresponds to $0 \leq |h| \leq 1 + h_p$. It is worth noting that the first solution in Eqs. (10) corresponds to the minimum of interaction energy for any value of the magnetic field h , while the third solution corresponds to the maximum of energy for $0 \leq |h| \leq 1 + h_p$ (Fig. 2).

According to Ref. [39], a particular phase can be considered stable in a certain range of the field h , provided the following conditions are obeyed:

$$\frac{\partial^2 U_0}{\partial \theta^2} > 0, \quad \frac{2}{\sin^2 \theta} \left[\frac{\partial^2 U_0}{\partial \theta^2} \frac{\partial^2 U_0}{\partial \varphi^2} - \left(\frac{\partial^2 U_0}{\partial \theta \partial \varphi} \right)^2 \right] > 0. \quad (11)$$

When one of these expressions turns to zero, with a consequent change of sign, the corresponding phase becomes unstable. Substitution of the solutions (10) into Eqs. (11) allows one to determine the conditions of the system stability loss (for certain values of φ) for the states, which are odd with respect to the magnetic field, i.e., for the states U_{01} and U_{02} . The phases U_{03} and U_{04} (even at nonzero h) are unstable in any case. This indicates on the possibility of spin re-orientation leading to transitions between the existing phases under applied magnetic fields $0 \leq h \leq 1$ or $1 \leq |h| \leq 1 + h_p$.

The boundary corresponding to the transitions between two phases is defined by the following equations:³⁹

$$\frac{\partial U_0}{\partial \theta} = 2 \sin \theta [Z(\varphi) \cos \theta + h] = 0, \quad \frac{\partial^2 U_0}{\partial \theta^2} = 2 [Z(\varphi) \cos 2\theta + h \cos \theta] = 0. \quad (12)$$

As the single solution of Eq.(12) coincides with the first solution in (10), it means that $\theta = 0$, $\varphi = 0.5 \arccos[-2(h+1)/h_p - 1]$ for $-(1+h_p) \leq h \leq -1$ with $U_{01} = -2h$ and $\theta = \pi$, $\varphi = 0.5 \arccos[2(h-1)/h_p - 1]$ for $1 \leq h \leq 1 + h_p$ with $U_{02} = 2h$ describe the lines of the second order phase transition,³⁹ in accordance with the Landau theory.⁴⁰

B. Constant energy solutions

Using Eqs. (5) and (6), we find that the variation of $U_0(\theta, \varphi)$ with time obeys the following equation:

$$\frac{\partial U_0(\theta, \varphi)}{\partial \tau} = -2 \sin^2 \theta \left\{ \alpha [(Z(\varphi) \cos \theta + h)^2 + (0.5h_p \sin 2\varphi + h_s)^2] + h_s [Z(\varphi) \cos \theta + h - \alpha (0.5h_p \sin 2\varphi + h_s)] \right\}. \quad (13)$$

From this follows that the potential energy of the system is an integral of motion [$U_0(\theta, \varphi) \equiv U_0 = \text{const}$] when

both $\alpha = 0$ and $h_s = 0$, which allows to transform Eq. (6) to the form

$$\frac{\partial \varphi}{\partial \tau} = \mp [h^2 - U_0 Z(\varphi) + Z(\varphi)^2]^{1/2}, \quad Z(\varphi) \cos \theta + h = -\frac{\partial \varphi}{\partial \tau}. \quad (14)$$

The "+" and "-" signs on the right-hand-side correspond to the two possible solutions for $\cos \theta$ from Eq. (5) at $U_0 = \text{const}$.

Equations (14) have real solutions only when

$$h^2 + Z(\varphi)^2 \geq U_0 Z(\varphi), \quad -1 \leq \cos \theta = -\frac{1}{Z(\varphi)} \left(\frac{\partial \varphi}{\partial \tau} + h \right) \leq 1. \quad (15)$$

The analysis of condition (15) shows that the solutions of Eqs. (14) exist for $|2h| < U_0 < U_{03}$ and $U_{03} < U_0 < U_{04}$, when it can be expressed by the Jacoby elliptic functions.⁴¹ However, if the interaction energy U_0 coincides with the energy of one of the equilibrium states (10), the solutions can be simplified to the inverse trigonometric or exponential functions. In particular, for the case of $U_0 = U_{01,2} = \pm 2|h|$, the solutions of Eqs. (14) are

$$\varphi = \mp \arctan \left[\sqrt{\xi/\zeta} \tanh(\sqrt{\zeta \xi} \tau) \right], \quad \cos \theta = \pm \left[1 - 2|h| \frac{\zeta + \xi \tanh^2(\sqrt{\zeta \xi} \tau)}{\zeta(1 + h_p) + \xi \tanh^2(\sqrt{\zeta \xi} \tau)} \right], \quad (16)$$

$$\xi \equiv (1 + h_p - |h|), \quad \zeta \equiv |h| - 1.$$

Here, the upper sign corresponds to the interval of $1 < h \leq 1 + h_p$, while the lower one is for the interval of $-(1+h_p) \leq h < -1$. When deriving Eq. (16) we assumed the integration constant $\tau_0 = 0$. Note that for $|h| \rightarrow 1$, the values of φ and $\cos \theta$ tend to the finite limits

$$\varphi_{|h \rightarrow 1} = \mp \arctan(h_p \tau), \quad \cos \theta_{|h \rightarrow 1} = \pm \left(-1 + \frac{2h_p}{1 + h_p + h_p^2 \tau^2} \right). \quad (17)$$

It is important to note, that apart from the states described by Eq. (16), there also exists the state with $\cos \theta = -1$ for arbitrary φ and $h > 0$, and the state with $\cos \theta = 1$ for $h < 0$. As follows from (17), if we neglect the plane anisotropy ($h_p = 0$) or take the limit of $\tau \rightarrow \infty$, Eq. (16) for $\cos \theta$ gives the independent on φ expressions mentioned above. In other words, Eqs. (16) and (17) prove that along the lines corresponding to the phase transitions of the second type, there are two possible solutions for the longitudinal magnetization component: a constant one, and a periodic solution with a complex time dependence. In particular, for $|h| > 1$ it is characterized by the cyclic frequency

$$\omega(h_p, h) = [(|h| - 1)(1 + h_p - |h|)]^{1/2}. \quad (18)$$

It is worth noting that Eq. (16) for $\varphi(\tau)$ and Eq. (18) almost coincide with similar expressions for $\varphi(\tau)$ and frequency ω_p from Ref. [20], if one transforms the field interval from $h > -1$ to $1 \leq |h| \leq 1 + h_p$ considered here.

When $U_0 = U_{03,4}$ the solution of (14) has the form:

a) for the case $U_0 = U_{03}$:

$$\sin^2 \varphi = [k'^2 \cot^2 (k' h_p (\tau - \tau_0)/k) - k^2]^{-1}, \quad (19)$$

$$Z(\varphi) \cos \theta_{1,2} = -h \pm \sqrt{(Z(\varphi) - 1)(Z(\varphi) - h^2)},$$

where $k^2 = h_p/(1 + h_p - h^2)$ and $k'^2 = 1 - k^2$.

b) for the case $U_0 = U_{04}$ and $h > \sqrt{1 + h_p}$:

$$\begin{aligned} \cos^2 \varphi &= (A^2 - 1) \frac{\tan^2 [h_p (\tau - \tau_0)/A]}{A^2 \tan^2 [h_p (\tau - \tau_0)/A] + 1}, \\ Z(\varphi) \cos \theta_{1,2} &= -h \pm (1 + h_p)^{-1/2} \\ &\times \sqrt{(1 + h_p - Z(\varphi))(h^2 - (1 + h_p)Z(\varphi))}, \end{aligned} \quad (20)$$

where $A^2 = h_p(1 + h_p)/[(1 + h_p)^2 - h^2] > 1$, and the expression for $Z(\varphi)$ is given by Eq. (2). The integration constant τ_0 in Eqs. (19) and (20) can be defined from the initial conditions. The comparison of formulas (17), (19) and (20) proves that the magnetization dynamics corresponding to the equilibrium energy is expressed with the complex functions of h and h_p , depending on the form of solutions (10).

C. Analytical solutions in the presence of spin current

Let us now turn back to the discussion of the effect of spin current. It is quite natural to expect that the spin current can affect the system in a way similar to that of an external magnetic field. In a general case, the influence of spin current on the magnetization dynamics can be studied only by the numerical integration of Eqs. (6). This will be presented later. Below we consider three particular cases of $h_s \neq 0$, for which some analytical solutions can be derived.

The simplest case is the one with $\alpha = 0$ and $h = 0$, when Eqs. (6) transform to

$$\begin{aligned} \frac{\partial \theta}{\partial \tau} &= -\left(\frac{1}{2} \sin 2\varphi + h_s\right) \sin \theta, \\ \frac{\partial \varphi}{\partial \tau} &= -Z(\varphi) \cos \theta. \end{aligned} \quad (21)$$

Excluding the time variable, the above system of two equations can be reduced to a single equation with the corresponding solution

$$\theta = \arcsin [U_0(\varphi)/Z(\varphi)]^{1/2}, \quad (22)$$

where

$$U_0(\varphi) = \exp\left(-\frac{2h_s \arctan(\sqrt{1 + h_p} \cot \varphi)}{\sqrt{1 + h_p}}\right). \quad (23)$$

The integration constant in Eq. (22) was determined from the condition that $\theta = \pi/2$ corresponds to $\varphi = \pi/2$.

Substituting Eq. (22) into Eqs. (21) and (5), we obtain

$$\frac{\partial \varphi}{\partial \tau} = -Z(\varphi) \left[1 - \frac{U_0(\varphi)}{Z(\varphi)}\right]^{1/2}. \quad (24)$$

It is obvious that the solution of Eq. (24) can be found only by numerical methods. However, some analytical results are achievable regarding the magnitude and sign of h_s . Equation (24) can have real solutions only when

$$\frac{\sqrt{1 + h_p} \ln Z(\varphi)}{2 \arctan(\sqrt{1 + h_p} \cot \varphi)} \geq -h_s. \quad (25)$$

If $h_s > 0$, the condition (25) is automatically fulfilled. With increasing spin current, the variables $\varphi(\tau)$, $\theta(\tau)$ and $U_0(\tau)$ relax to their equilibrium values, corresponding to the limiting case of $h_s \rightarrow \infty$:

$$\begin{aligned} \varphi &= -\arctan \left[\sqrt{1 + h_p} \cot \left(\sqrt{1 + h_p} \tau - \frac{\pi}{2} \right) \right], \\ \sin \theta &= 0, \quad U_0 = 0. \end{aligned} \quad (26)$$

The integration constant for $\varphi(\tau)$ in Eq. (26) was chosen to keep $\varphi(\tau = 0) = 0$. It is important to note that the nature of the solution (26) coincides with the first solution in Eq. (10).

For $h_s < 0$ and for certain values of spin current, Eq. (25) is no longer valid and the system cannot be integrated. When the left and right sides of Eq. (25) are equal, the system exists in the state

$$\sin \theta = 1, \quad \varphi = 0, \quad U_0 = 1, \quad (27)$$

which coincides with the second solution in Eq. (10).

Therefore, when no magnetic field is applied, the spin current can excite the magnetic system, which in turn may relax either to the first or to the second state described by Eqs. (10), depending on the sign of h_s . In other words, the behavior of the system depends on both direction and magnitude of the spin current. One has to pay special attention to the exponential character of this dependence, because a comparatively small change of h_s in certain direction can result in a significant change of the magnetization orientation and of the interaction energy. It is also worth noting that the dependence of the magnetization components and the interaction energy on the applied magnetic field is much weaker, being linear or quadratic in h .

The second case, where some analytical solutions are possible, is the situation with $h_p = 0$. Equations (6) can be then rewritten for $m_z = \cos \theta$ as

$$\begin{aligned} \frac{\partial m_z}{\partial \tau} &= \alpha(1 - m_z^2)(m_z + h + h_s/\alpha) \\ \frac{\partial \varphi}{\partial \tau} &= -(m_z + h - \alpha h_s) \end{aligned} \quad (28)$$

It can be shown that for the case $\alpha h + h_s \neq \pm \alpha$, the solution of Eq. (28) has the following form

$$\frac{1 - m_z^2}{(m_z + \beta)^2} \left(\frac{1 + m_z}{1 - m_z} \right)^\beta$$

$$= \frac{1 - m_{z0}^2}{(m_{z0} + \beta)^2} \left(\frac{1 + m_{z0}}{1 - m_{z0}} \right)^\beta e^{-2\alpha(1-\beta^2)\tau}, \quad (29)$$

$$\varphi(\tau) = \varphi_0 - (h - \alpha h_s)\tau - \int_0^\tau m_z(\tau) d\tau,$$

where $\varphi(0)$ is the initial value of the angular variable and

$$\beta = h + \frac{h_s}{\alpha}. \quad (30)$$

Equations (29) and (30) represent a generalization of Eqs. (22) and (23) from Ref. [20] to the case of arbitrary θ . As follows from Eq. (29), in the stationary case ($\tau \rightarrow \infty$) and for vanishing easy-plane anisotropy, the system turns to the state with $m_z = \cos\theta_0 = -1$ in a complicated manner. At the initial time, the interaction energy has a jump $\partial U_0(h_p = 0)/\partial\tau|_{\tau=0} = -2\alpha\beta h$; further on, depending on the sign of β , it increases or decreases in an oscillatory manner to reach the value of $\partial U_0(h_p = 0)/\partial\tau|_{\tau \rightarrow \infty} = 0$.

Some analytical solutions can also be obtained for the stationary situations, when Eqs. (6) can be transformed into a trigonometric form with the general periodic solutions θ_0 and φ_0 given by

$$\begin{aligned} \sin 2\varphi_0 &= -2h_s/h_p, \\ \cos \theta_0 &= -h/Z(\varphi_0). \end{aligned} \quad (31)$$

The invariance conditions (7) allow to select only two independent stationary states from those described by Eq. (31):

$$\begin{aligned} \varphi_{01} + \varphi_{02} &= \pi/2, \\ \cos \varphi_{02} &= -\text{sign } h_s \sqrt{\frac{1}{2} \left(1 - \sqrt{1 - 4h_s^2/h_p^2} \right)}, \\ \sin \varphi_{02} &= \sqrt{\frac{1}{2} \left(1 + \sqrt{1 - 4h_s^2/h_p^2} \right)}, \\ \sin \varphi_{01} &= \cos \varphi_{02}, \quad \cos \varphi_{01} = \sin \varphi_{02}, \\ \cos \theta_{01,2} &= -h/Z(\varphi_{01,2}). \end{aligned} \quad (32)$$

As follows from Eqs. (32), the stationary states are possible only for h_s satisfying the condition $|h_s| \leq 0.5h_p$. At the same time, the positive or negative value of the longitudinal magnetization vector component is determined by the orientation of external magnetic field, being independent of the angle between the spin current and e_z . It is important to note that the stationary states described by Eq. (32) are characterized by the potential energy of Eq. (5), which is an integral of motion with the corresponding eigenvalues

$$U_{S01,2} = Z(\varphi_{01,2}) + h^2/Z(\varphi_{01,2}). \quad (33)$$

The differences between the equilibrium energies $U_{03} = 1 + h$ and $U_{04} = 1 + h_p + h^2/(1 + h_p)$ and these stationary states $U_{S01,2}$ are

$$\Delta U_{01}|_{0 \leq |h| \leq 1+h_p} = U_{04} - U_{S01}$$

$$= y - \frac{yh^2}{(1+h_p)(1+y+h_p\sqrt{1-x^2})},$$

$$\Delta U_{02}|_{0 \leq |h| \leq 1} = U_{S02} - U_{03} = y - \frac{yh^2}{1+y}, \quad (34)$$

$$x \equiv \left| \frac{2h_s}{h_p} \right|, \quad y \equiv \frac{1}{2} h_p \left(1 - \sqrt{1-x^2} \right).$$

Therefore, Eqs. (32) to (34) demonstrate that neither stationary states nor the corresponding energies depend on the damping coefficient α , as they are only determined by h , h_p and h_s . From Eq. (34) follows that for $h_s = 0$, the stationary state U_{S01} coincides with U_{04} , and U_{S02} with U_{03} . Under the influence of spin current, the state U_{04} shifts towards the lower energy and becomes more thermodynamically stable transforming into the state U_{S01} , while the state U_{03} increases in energy and transforms into the state U_{S02} . As follows from Eq. (31), the relative position of both stationary states on the energy scale could be then changed in controllable way by means of a proper choice of h and h_s .

D. Stability of the equilibrium and stationary states

To investigate the stability of equilibrium (10) or stationary (32) solutions, we subject them to small perturbations

$$\theta = \theta_i + \delta\theta_i, \quad \varphi = \varphi_i + \delta\varphi_i, \quad (i = e \text{ or } 0) \quad (35)$$

with $\delta\theta_i \ll \theta_i$, $\delta\varphi_i \ll \varphi_i$. Physically, such perturbations can have quite different origin: they can be caused either by a non-homogeneity of the sample, presence of contacts, fluctuations of the temperature or external fields,⁴² etc. Substituting (35) into (6) and performing a standard linearization procedure over small perturbations,³⁴ one obtains the dynamic matrix \mathbf{a} with the corresponding eigenvalues

$$\lambda_{1,2} = 0.5 \left(a_{11} + a_{22} \pm \sqrt{(a_{11} - a_{22})^2 + 4a_{12}a_{21}} \right) \quad (36)$$

and the matrix elements a_{ij}

$$\begin{aligned} a_{11} &= -\cos \theta_1 \{ \alpha [Z(\varphi_i) + h] + 0.5h_p \sin 2\varphi_i + h_s \} \\ &\quad + \alpha Z(\varphi_i) \sin^2 \theta_i, \\ a_{12} &= h_p \sin \theta_i (\alpha \cos \theta_i \sin 2\varphi_i - \cos 2\varphi_i), \\ a_{21} &= \sin \theta_i Z(\varphi_i), \\ a_{22} &= h_p (\cos \theta_i \sin 2\varphi_i + \alpha \cos 2\varphi_i). \end{aligned} \quad (37)$$

After substituting the solutions (10) into Eq. (37) and then into Eq. (36), one obtains three different solutions:

a) for the state with $\sin \theta_e = 0$, φ_e arbitrary:

$$\begin{aligned} \lambda_1 &= \mp \{ \alpha [Z(\varphi_e) + h] + 0.5h_p \sin 2\varphi_e + h_s \}, \\ \lambda_2 &= h_p (\pm \sin 2\varphi_e + \alpha \cos 2\varphi_e), \end{aligned} \quad (38)$$

with the upper and lower signs corresponding to $\theta_e = 0$ and $\theta_e = \pi$, respectively.

b) for the state with $\cos \theta_e = -h$, $\varphi_e = \pi/2$

$$\lambda_{1,2} = \frac{1}{2} [h h_s + \alpha(1 + h - h_p) \pm \sqrt{[h h_s + \alpha(1 + h + h_p)]^2 + 4h_p(1 - h^2)}] \quad (39)$$

c) for the state with $\cos \theta_e = -h/(1 + h_p)$, $\varphi_e = 0$:

$$\lambda_{1,2} = \frac{0.5}{1 + h_p} \left[h h_s + \alpha(1 + h_p)(1 + 2h_p + h) \pm \{ [h h_s + \alpha(1 + h_p)(1 + h)]^2 - 4h_p(1 + h_p)[(1 + h_p)^2 - h^2] \}^{1/2} \right], \quad (40)$$

The solutions of the characteristic equation, corresponding to the stationary states (32), are rather complicated and we have calculated them numerically. It is worth noting that the solutions (38) and (39) are real ($\lambda_1 > 0$ and $\lambda_2 < 0$) – also for the stationary state (θ_{02} , φ_{02}). In turn, the solutions (40) are complex-conjugated ($\lambda_{1,2} = \lambda_r \pm i\lambda_{im}$), including the case of stationary state (θ_{01} , φ_{01}).

The stability of the equilibrium or stationary states can be estimated using different stability criteria. In our case, we apply the method of Lyapunov,⁴³ evaluating the stability from the signs of λ_1 and λ_2 , as well as the criteria of Gurvitz,^{44,45} taking into account the relations between the matrix elements a_{ij} . In particular, according to Gurvitz, the sufficient conditions for stability of the system under consideration are

$$a_{11} + a_{22} < 0, \quad a_{11}a_{22} > a_{12}a_{21}. \quad (41)$$

If λ_1 and λ_2 (see Eq. (36)) are known, the solutions $\theta(\tau)$ and $\varphi(\tau)$ have the following form⁴³

(a) for the case of real λ_1 and λ_2 :

$$\begin{aligned} \theta(\tau) &= \theta_i + C_{11}e^{\lambda_1\tau} + C_{12}e^{\lambda_2\tau}, \\ \varphi(\tau) &= \varphi_i + C_{21}e^{\lambda_1\tau} + C_{22}e^{\lambda_2\tau}, \end{aligned} \quad (42)$$

(b) for the complex-conjugate λ_1 and λ_2 :

$$\begin{aligned} \theta(\tau) &= \theta_i + 2 [D_{11} \cos(\lambda_{im}\tau) - D_{12} \sin(\lambda_{im}\tau)] e^{\lambda_r\tau}, \\ \varphi(\tau) &= \varphi_i + 2 [D_{21} \cos(\lambda_{im}\tau) - D_{22} \sin(\lambda_{im}\tau)] e^{\lambda_r\tau}. \end{aligned} \quad (43)$$

Here C_{ij} and D_{ij} are the integration constants, which are generally determined from the relevant boundary conditions. The latter ones can be written as

$$\begin{aligned} \theta(\tau)|_{\tau=0} &= \theta_i + 2\pi, & \varphi(\tau)|_{\tau=0} &= \varphi_i + \pi, \\ \frac{\partial\theta(\tau)}{\partial\tau} \Big|_{\tau=0} &= 2 \frac{\partial\varphi(\tau)}{\partial\tau} \Big|_{\tau=0} & &= -2\pi|\lambda_2| \end{aligned} \quad (44)$$

for real λ_1 and λ_2 , and

$$\begin{aligned} \theta(\tau)|_{\tau=0} &= \theta_i, & \varphi(\tau)|_{\tau=0} &= \varphi_i, \\ \frac{\partial\theta(\tau)}{\partial\tau} \Big|_{\tau=0} &= 2 \frac{\partial\varphi(\tau)}{\partial\tau} \Big|_{\tau=0} & &= -2\pi|\lambda_{im}| \end{aligned} \quad (45)$$

for complex-conjugate λ_1 and λ_2 . Equations (42) and (43) can be rewritten as

$$\begin{aligned} \theta_2(\tau) &= \theta_{i2} + 2\pi \exp(\lambda_2\tau), \\ \varphi_2(\tau) &= \varphi_{i2} + \pi \exp(\lambda_2\tau) \end{aligned} \quad (46)$$

for real λ_1 and λ_2 , and

$$\begin{aligned} \theta_1(\tau) &= \theta_{i1} + 2\pi \exp(\lambda_r\tau) \sin(\lambda_{im}\tau), \\ \varphi_1(\tau) &= \varphi_{i1} + \pi \exp(\lambda_r\tau) \sin(\lambda_{im}\tau) \end{aligned} \quad (47)$$

for complex conjugated λ_1 and λ_2 . As follows from Eqs. (46) and (47), the functions $\theta(\tau)$ and $\varphi(\tau)$ can have either monotonic or oscillatory character, with the characteristics depending on the control parameters in a rather complex way, which can be investigated by numerical calculations described later.

E. Phase averaging

Let us come back to Eq. (13) describing the time variation of the interaction energy. Using Eqs. (6), one can rewrite this equation in the form

$$\begin{aligned} 2h_s \sin^2 \theta \frac{\partial\varphi}{\partial\tau} - \frac{\partial U_0}{\partial\tau} &= 2\alpha \sin^2 \theta \\ \times \{ [Z(\varphi) \cos \theta + h]^2 + (0.5h_p \sin 2\varphi + h_s)^2 \}. \end{aligned} \quad (48)$$

On the right side of Eq. (48) there is a positive quadratic form with a constant magnitude under any transformation of the coordinate system. Hence, when the spin current is absent, the energy $U_0(\theta, \varphi, \tau)$ decreases with time, i.e., the system tends to an equilibrium state. If $h_s \neq 0$, the variation of energy $\partial U_0/\partial\tau$ can be either positive or negative, depending on the sign and magnitude of the first term on the left side of Eq. (48). As $\partial\varphi/\partial\tau$ is determined by h_s for the fixed values of h_p and α , it is natural that $\partial U_0/\partial\tau$ also depends mainly on the direction and magnitude of the spin current.

To reveal the exact form of this dependence, one has to average Eq. (48) over the phase. When performing such an averaging, we take into account the periodicity of Eq. (48) and also the invariance relations (7). For the averaging procedure we will use two possible approaches: without any weighting coefficients⁴⁴

$$\langle f \rangle \equiv \langle f(\theta, \varphi) \rangle = \frac{1}{\pi^2} \int_0^\pi \int_0^\pi f(\theta, \varphi) d\theta d\varphi, \quad (49)$$

and with weighting coefficients^{44,46}:

$$\langle f \rangle \equiv \langle f(\theta, \varphi) \rangle = \frac{1}{2\pi} \int_0^\pi \int_0^\pi f(\theta, \varphi) \sin \theta d\theta d\varphi. \quad (50)$$

Substituting (48) into (49) and (50), one obtains

a) for the averaging procedure (49)

$$-\left[h\frac{h_s}{\alpha} + \frac{1}{\alpha}\left\langle\frac{\partial U_0}{\partial\tau}\right\rangle\right] = h^2 + \frac{1}{4}\left(1 + \frac{h_p}{2}\right)^2 + \frac{5h_p^2}{32}, \quad (51)$$

b) for the averaging procedure (50)

$$-\left[\frac{4h\cdot h_s}{3\alpha} + \frac{1}{\alpha}\left\langle\frac{\partial U_0}{\partial\tau}\right\rangle\right] = \frac{4}{3}\left[h^2 + \frac{(1+h_p+h_p^2)}{5}\right]. \quad (52)$$

First of all, it is necessary to emphasize that the expressions (51) and (52) have the same functional dependence on h and h_s , correlating well with the invariance upon simultaneous replacement $h \rightarrow -h$ and $h_s \rightarrow -h_s$ (see Eq. (8)). As one can see, the right hand sides of the obtained formulas do not include h_s . This means that when the external magnetic field and the spin current have the same direction, the average energy can decrease faster than in the case of $h_s = 0$. For antiparallel h and h_s , the average $\langle\partial U_0/\partial\tau\rangle$ can be negative, zero, or can become positive – but its absolute value is always smaller than $|h\cdot h_s|$ to obey Eqs. (51) or (52). It is worth noting that the approximation $\theta \ll 1$, used in [20], leads to the violation of the symmetry condition (8), which is also reflected in the averaging formula (49) for $\langle\partial U_0/\partial\tau\rangle$:

$$\begin{aligned} -\left[\frac{h_s}{\alpha}\left(1 + \frac{h_p}{2} + h\right) + \frac{1}{2\alpha\theta_0^2}\left\langle\frac{\partial U_0}{\partial\tau}\right\rangle_{|\theta\ll 1}\right] \\ = \left(1 + \frac{h_p}{2} + h\right)^2 + \frac{h_p^2}{4}. \end{aligned} \quad (53)$$

The averaging procedure (50) in the given approximation should be changed to

$$\langle f \rangle_{|\theta\ll 1} = \frac{1}{\pi\theta_0} \int_0^{\theta_0} \int_0^\pi \theta f(\theta, \varphi) d\theta d\varphi, \quad (54)$$

leading to two times greater coefficient at $\langle\partial U_0/\partial\tau\rangle$ in (53).

The difference between the expression (53) and the corresponding formula (16) from Ref. [20] is caused by the fact that we take into account the quadratic term in the expansion $\cos\theta|_{\theta\ll 1} \approx 1 - \theta^2/2$, which was neglected in Ref. [20].

III. RESULTS OF NUMERICAL CALCULATIONS AND THEIR DISCUSSION

Using the formulas presented above, the magnetization dynamics of a single-domain ferromagnet can be investigated as a function of the control parameters: α , h_p , h_s and h . In our calculations, the number of control parameters was reduced to h and h_s by assuming $\alpha = 0.005$ (see Ref. [11]) and $h_p = 5$ (as in Ref. [20]).

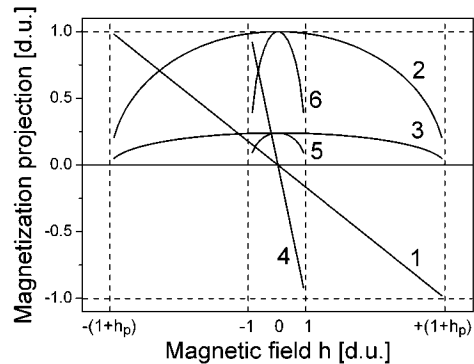


FIG. 3: Field dependence of the stationary magnetic moment components. The curves labelled with 1, 2 and 3 correspond respectively to m_{z1} , m_{x1} and $40m_{y1}$; whereas the curves 4, 5 and 6 represent m_{z2} , $40m_{x2}$, and m_{y2} . (The curves 3 and 5 have been multiplied by the factor of 40.)

A. Analysis of equilibrium and stationary states

Let us discuss first the dependence of stationary magnetization states on the parameters h and h_s . Figure 3 shows the magnetic field dependence of $m_x = \sin\theta_0 \cos\varphi_0$, $m_y = \sin\theta_0 \sin\varphi_0$, and $m_z = \cos\theta_0$ components of a unit magnetization vector \mathbf{m} , corresponding to the stationary states (32). All other control parameters are kept constant in the calculations, namely $\alpha = 0.005$, $h_p = 5$ and $h_s = -0.03$. As one can see, there is a range of magnetic field, where the magnetization components are non-zero for both stationary states. It is important to emphasize that the limiting field values $\pm h_{lim}$ depend on h_s/h_p for the stationary state $(\theta_{01}, \varphi_{01})$, remaining practically independent on h_s/h_p for the state $(\theta_{02}, \varphi_{02})$ with $h_{lim} = \pm 1$. In both cases, the longitudinal component m_z varies linearly with magnetic field, whereas the transverse components $m_x < m_y$ have a non-linear field dependence. For better visual presentation of the data, the curves 3 and 5 in Fig. 3 have been multiplied by the factor of 40.

The solutions of the characteristic equations for the equilibrium [(39), (40)] and stationary [(32), (36), and (37)] states are plotted in Fig. 4 as a function of h . The solutions corresponding to the stationary state $(\theta_{01}, \varphi_{01})$ are complex conjugated (curves 1, 2 and 3), whereas the ones corresponding to $(\theta_{02}, \varphi_{02})$ are real numbers of opposite signs (curves 5 and 6). It is worth noting that the real part λ_r (curves 1 and 3) for the stationary state $(\theta_{01}, \varphi_{01})$ can be positive (area A), negative (area D) or equal to zero (point C).

As concerns solutions of the characteristic equation for the equilibrium state (39), we note that the curves 5' and 6' in Fig. 4 practically coincide with the solutions for the stationary states $(\theta_{02}, \varphi_{02})$ (curves 5 and 6). For the state (40), only the imaginary parts of the solutions (curves 2' and 4') coincide with the imaginary parts describing the state $(\theta_{01}, \varphi_{01})$ (curves 2 and 4), whereas the

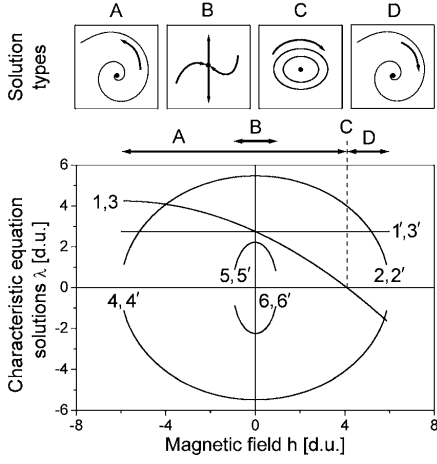


FIG. 4: Magnetic field dependence of the characteristic equation solutions: real (curves 1 and 3) and imaginary (curves 2 and 4) parts of λ_1 , real parts of λ_2 (curves 5 and 6). Stationary states: curves 1 – 6, equilibrium states: curves 1' – 6'. The curves 1,3 and 1', 3' are multiplied by the factor of 100.

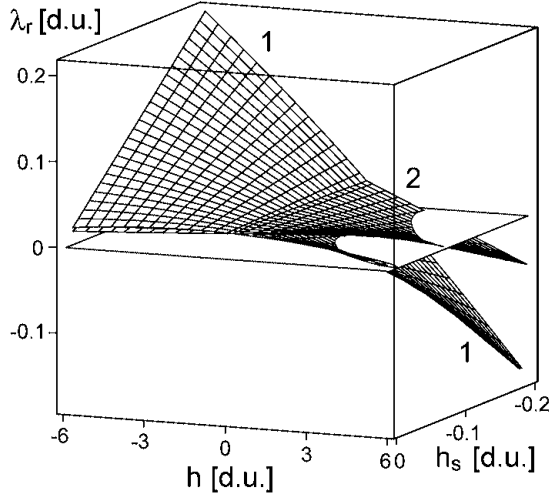


FIG. 5: The real part of the characteristic equation solution as a function of h and h_s : 1 – stationary state, 2 – equilibrium state.

real parts of these solutions differ significantly (curves 1', 3' and 1, 3 in Fig. 4 are scaled by the factor of 100 for better visual presentation). It is important that for the given values of the control parameters, the real part of (40) does not depend on h . However, if the control parameters are changed in a sufficiently wide range, the real parts of the solutions (40) and $(\theta_{01}, \varphi_{01})$ behave similarly (Fig. 5). The difference between them is seen in the intersection of the surfaces $\lambda_{ri} = f(h, h_s)$, ($i = e, 0$) with the $\lambda_r = 0$ plane, which for the stationary state takes place for weaker magnetic fields.

According to the classification of specific points describing the motion in the vicinity of equilibrium states,⁴³ the solution $(\theta_{02}, \varphi_{02})$ corresponds to a saddle point

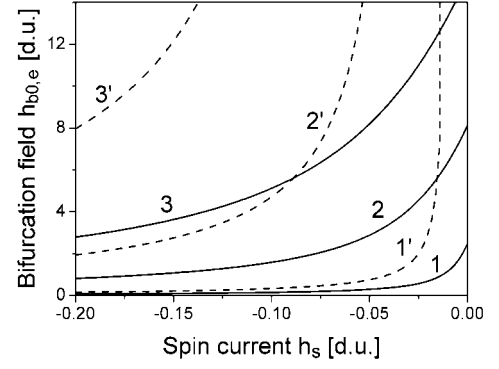


FIG. 6: Bifurcation diagram of neutral stability for stationary (solid curves) and equilibrium (dashed curves) states for $\alpha = 0.005$ and different h_p : 1 and 1' correspond to $h_p = 1$; 2 and 2' correspond to $h_p = 5$; 3 and 3' correspond to $h_p = 10$.

(Fig. 4, B) with two attracting equilibrium states. The second stationary state $(\theta_{01}, \varphi_{01})$ has a broader variety of possible motion types: unstable focus (Fig. 4, A), stable focus (Fig. 4, D), and stable center (Fig. 4, C). It is interesting to note that the point, where the stable center appears is located on the boundary between the intervals of stable and unstable foci. Therefore, the condition of reaching the stable center, $\lambda_r(h_b) = 0$, determines the bifurcation point h_b (the boundary of neutral stability³⁴) as

$$h_{b0} = \frac{h_s}{\alpha} + \sqrt{\left(\frac{h_s}{\alpha}\right)^2 + \left(1 + \frac{h_p}{2} + \sqrt{\varpi}\right)^2 - \frac{\varpi}{4}}, \quad (55)$$

where $\varpi \equiv h_p^2 - 4h_s^2$.

As follows from Eq. (55), with h_s decreasing from zero to $h_s = -h_p/2$, the value of h_b diminishes monotonously from $h_{b0}^{max} = \sqrt{(1+h_p)(1+2h_p)}$ to $h_{b0}^{min} = -(h_p/2\alpha) + \sqrt{(h_p/2\alpha)^2 + (1+0.5h_p)^2}$ (see Fig. 6). At the same time, h_{b0} shows a non-linear increase with the anisotropy h_p . It is worth noting that for the equilibrium state (40), the neutral stability field boundary h_{be} (Fig. 6, dashed lines) is determined from the expression,

$$h_{be} = -\frac{(1+h_p)(1+2h_p)}{h_s\alpha^{-1} + 1 + h_p}, \quad (56)$$

satisfying also the condition $h_{be} > h_{b0}$. In this way, (55) and (56) determine the system stability limits, as the corresponding states are stable when $h > h_{be}$ ($i = 0, e$) and unstable in the opposite case.

The two-dimensional plot of the energy of both U_{s01} and U_{s02} stationary states, calculated using (34), is presented in Fig. 7 for $0 \leq |h| \leq 1$ (state $(\theta_{02}, \varphi_{02})$) and for $0 \leq |h| \leq 6$ (state $(\theta_{01}, \varphi_{01})$); $0 \leq x \equiv |2h_s/h_p| \leq 1$. For $h = 0$ both surfaces merge, taking the energy value $U_{s0}(h = 0) = 1 + 0.5h_p$. With increasing h , the energy of the low-energy state U_{s02} increases slightly, but this increase is faster for larger values of the spin current h_s . Contrary, the changes of the high-energy state U_{s01} with

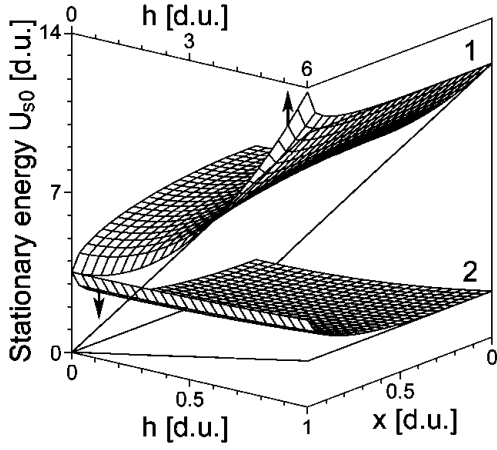


FIG. 7: Dependence of the stationary energy on h and $x \equiv |2h_s/h_p|$: 1 - U_{s01} , 2 - U_{s02} .

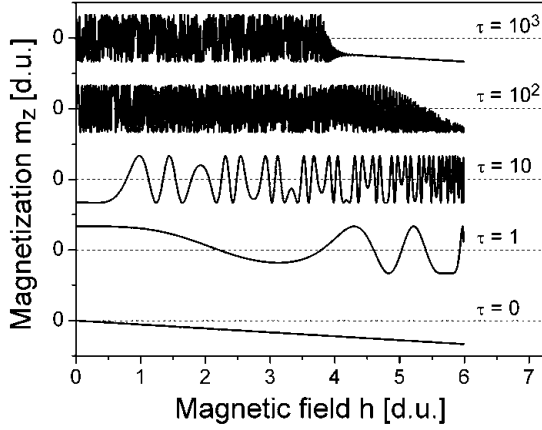


FIG. 8: Dependence of m_z on external magnetic field for the stationary state at different observation times.

increase of either h and h_s are significant, non-linear, and lead to much greater difference in the energy of the states U_{s01} and U_{s02} . Therefore, we will focus below on the non-stationary magnetization dynamics, corresponding to the excited state U_{s01} .

The time and field behavior of the longitudinal magnetization component m_z under small perturbations are illustrated in Figs. 8 and 9 for the stationary ($\theta_{01}, \varphi_{01}$) and equilibrium (U_{04}) states, using formulas (36), (37) and (47). At the initial moment ($\tau = 0$) and after a short period of time ($\tau = 1$), the changes of the m_z component with the increasing magnetic field are equal for both stationary and equilibrium states, but with a further increase of the observation time, the character of these curves becomes different, at first slightly ($\tau = 10$) and then significantly ($\tau \geq 10^2$). It is worth noting that the oscillations become chaotic, causing m_z to take random values in the range of $-1 \leq m_z \leq 1$. It is important that for $\tau \geq 10^3$ and $h > 4.2$ (Fig. 8), the perturbation of the state ($\theta_{01}, \varphi_{01}$) relaxes to the linear $m_z = f(h)$ de-

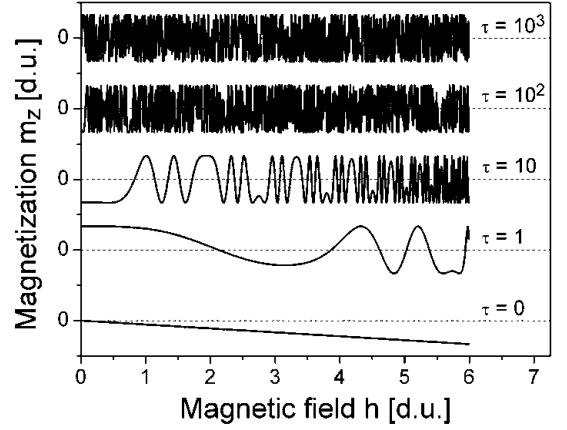


FIG. 9: Dependence of m_z on external magnetic field for the equilibrium state at different observation times.

pendence, comparable with Fig. 3 (curve 1), while the relaxation of equilibrium state (40) takes place for $\tau > 10^4$.

Therefore, under the influence of small perturbations, the high-energy stationary and equilibrium states of the ferromagnetic system in magnetic field are characterized with the complex temporal dynamics, which can be investigated in detail using the numerical methods to solve Eqs. (6).

B. Results of numerical modelling

The type of spin orientation in the system varies significantly with a change of the applied magnetic field. Our investigation reveals the presence of several oscillation regimes depending on the value of the applied magnetic field h . The set of differential equations (6) was solved numerically using the Runge-Kutta method of the fourth order.⁴⁹ This allows to observe the motion of the magnetization vector in the three-dimensional space, forming a phase portrait of the system. To determine the effect of magnetic field on switching between the states $m_z = \pm 1$, the magnetization vector was assumed to point down at the initial moment, i.e., $m_x = m_y = 0, m_z = -1$.

The most characteristic phase portraits of the system, shown in Fig. 10, were obtained for $h_s = -0.03$, $-5 \leq h \leq 15$, $\alpha = 0.005$, and $h_p = 5$. The density plot of m_z component versus applied field (Fig. 10(a)) features darker areas corresponding to the most frequent m_z values at a given magnetic field. The field dependence of the power spectral density $S(\omega)$ of the component m_z is given in Fig. 10(b), showing the peaks as dark areas. The precession velocity can be estimated from the trajectory tracing curve evolution,^{50,51} shown in Fig. 10(c). Here the dark areas correspond to the moments of time τ , when the vector connecting two consecutive phase points becomes parallel to the one between two initial points; the distance between two black stripes $\Delta\tau$ is inversely proportional to the velocity of the phase point. The

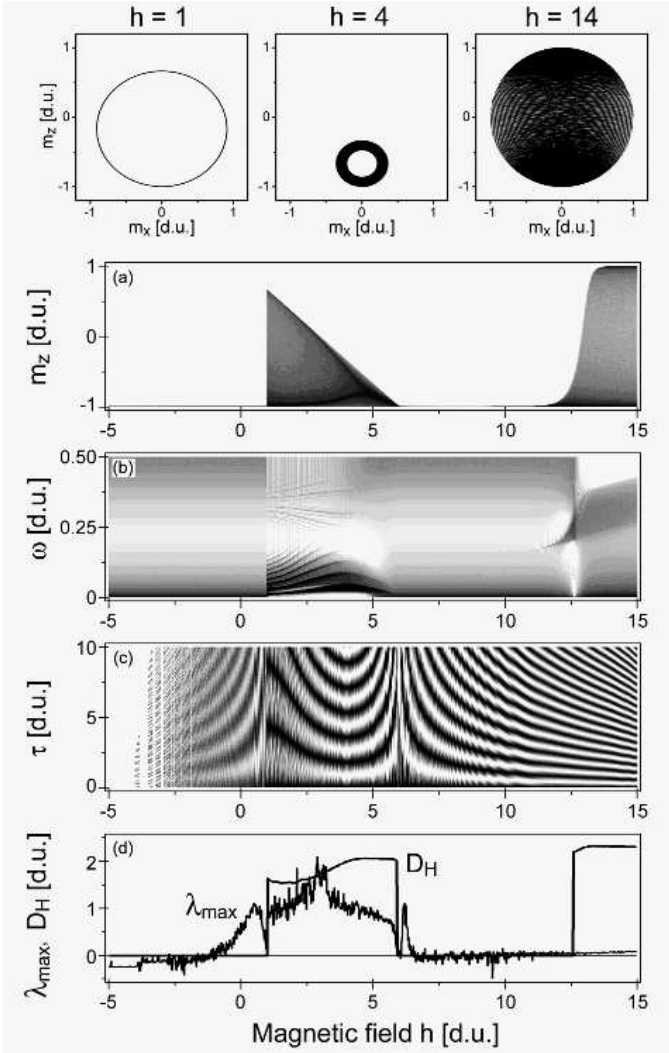


FIG. 10: Phase portraits and main system characteristics *vs* applied magnetic field: (a) m_z density plot, (b) m_z power spectral density $S(\omega)$, (c) evolution of trajectory tracing curve, and (d) Hausdorff dimension D_H and maximum Lyapunov exponent λ_{max} .

Hausdorff dimension D_H of the phase portrait and maximum Lyapunov exponent λ_{max} are shown in Fig. 10(d) for different values of the applied field.

For magnetic fields $h < 1$ the phase point remains in the vicinity of the ground state $m_z = -1$ during all the observation time, which is clearly seen at the density plot as the dark horizontal bottom line. The trajectory tracing curves allow to discern a negligibly small movement of the phase point characterized by a period increasing with the applied magnetic field. The tendency to instability is also notable from the λ_{max} curve reaching positive values. When the applied field h surpasses $h = 1$, the system switches to the magnetization precession mode, characterized by the periodic phase point orbit in m_x, m_z plane (Fig. 10, $h = 1$). The corresponding place of the density plot shows two darker branches, marking the upper and

lower limits of m_z values, which are contracting towards $m_z = -1$ with increasing magnetic field. Darkening of almost homogeneous gray area between these branches at higher h is caused by the limit cycle stability loss, visually observable as a phase trajectory broadening (Fig. 10, $h=4$). At a certain merging point of $h \approx 5$, the darker branches join together and the phase portrait of the system turns to the focus, i.e., the magnetization precession converges to a value close to the state $m_z = -1$.

It is worth noting that the $S(\omega)$ plot reveals several peaks corresponding to the harmonic oscillations in the limit cycle mode. The number of these peaks diminishes upon reaching the magnetic fields above which the phase portrait of the system turns into a focus. As can be deduced from the trajectory tracing plot, the initial shrinking of the limit cycle oscillation mode is accompanied by the precession frequency increase almost up to the merging point. The movement of the phase point becomes then slower for higher magnetic fields. The limit cycle stability loss and the corresponding increase of the phase portrait density could be clearly seen from the Hausdorff dimension curve, featuring a rapid increase from 1.55 to 2.05 before the merging point and almost no changes above it. The Lyapunov exponent has a noisy maximum at $h \approx 3$, revealing a return to the stable state upon switching to the converging magnetization precession mode.

It is worth noting that in the whole range of applied field, $6 < h < 11$, the magnetization vector is restricted to the closest vicinity of its ground state $m_z = -1$. At the same time, as it can be deduced from the trajectory tracing plot, the frequency of the phase point precession increases, and starting from $h \approx 11.1$ the system begins to tend to the upper state with $m_z = 1$ through the magnetization precession. The phase portrait corresponding to this oscillation mode represents a sphere formed by a tight spiral with Hausdorff density $D_H = 2.3$ (Fig. 10, $h=14$). It is worth noting a rather stable nature of such precession, described with almost zero values of λ_{max} .

A similar magnetization dynamics is also observed for different values of h_s , as it can be seen from Fig. 11, presenting several m_z density plots. In all the cases, the system under consideration does not leave the vicinity of the ground state $m_z = -1$ until the magnetic field overcomes the value $h = 1$. Above this point, it is possible to observe a magnetization vector precession to the state $m_z = 1$ for $h_s = 0$ and $h_s = -0.01$, while for higher negative spin current values, the system is switched to the limit cycle mode. From now on, the system evolution follows the same scenario with the limit cycle contracting into a focus. Depending on the spin current value, the system remains in the vicinity of the bottom ground state for different ranges of the applied field h . Starting from some threshold field, which increases with the absolute value of h_s , one can observe the switching of the system from the bottom to the upper ground state.

In the framework of our description, we have performed the averaging of the expression (48) over time according

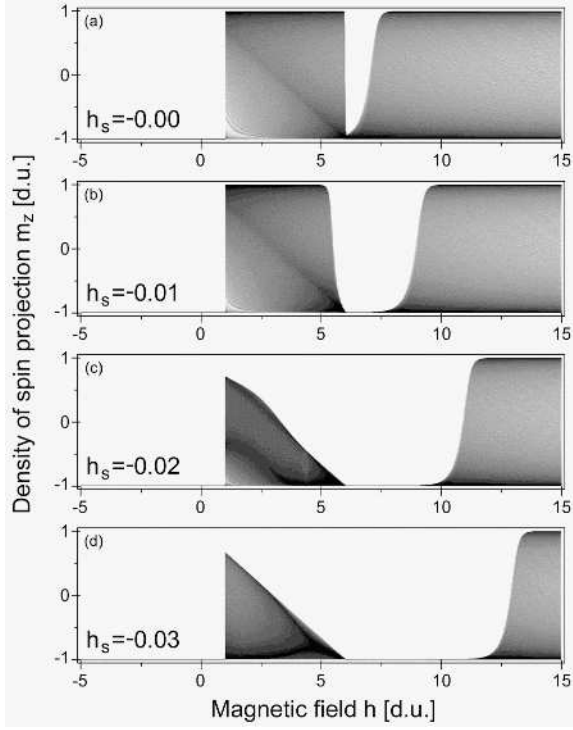


FIG. 11: The system evolution with the applied magnetic field h : m_z density plots for different values of the spin current.

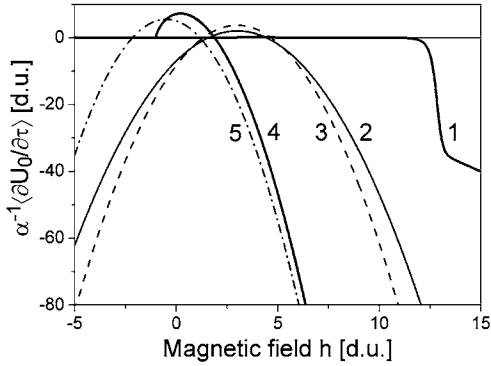


FIG. 12: Dependence of $\alpha^{-1}\langle\partial U_0/\partial\tau\rangle$ on the applied magnetic field for different averaging procedures: 1 - according to (57), 2 - from the formula (51), 3 - using (52), 4 - from (57), 5 - according to the formula (53).

to Ref. [46]:

$$\left\langle \frac{\partial U_0}{\partial \tau} \right\rangle = \lim_{T \rightarrow \infty} \frac{1}{T} \int_0^T \frac{\partial U_0(\tau)}{\partial \tau} d\tau, \quad (57)$$

where the value $\partial U_0/\partial\tau$ was calculated for $\theta(\tau)$ and $\varphi(\tau)$, determined from the numerical solution of Eqs. (6) using the Runge-Kutta method, and changing the condition $T \rightarrow \infty$ in (57) to $T \rightarrow T_{max}$, where T_{max} was selected from $\langle\partial U_0/\partial\tau\rangle$ saturation condition.

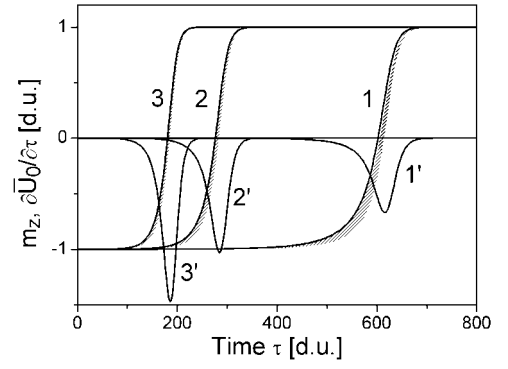


FIG. 13: Time evolution of m_z (curves 1, 2, 3) and $\partial\bar{U}_0/\partial\tau$ (curves 1', 2', 3'), calculated for $h_s = -0.03$ and different applied magnetic fields: 1,1' for $h = 11$; 2,2' for $h = 13$; 3,3' for $h = 15$.

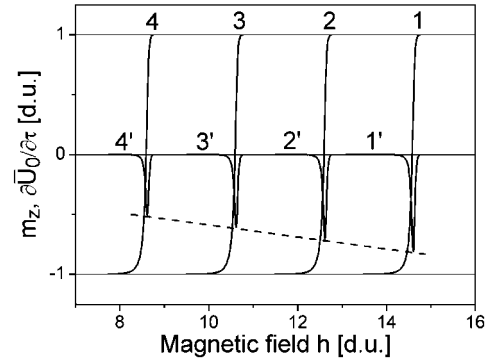


FIG. 14: Magnetization component m_z (curves 1-4) and $\partial\bar{U}_0/\partial\tau$ (curves 1'-4') as a function of magnetic field for $\tau = 800$ and different spin currents: 1,1' - for $h_s = -0.05$; 2,2' - for $h_s = -0.04$; 3,3' - for $h_s = -0.03$; 4,4' - for $h_s = -0.02$.

From the comparison of the curve 1 in Fig. 12, calculated according to formula (57), with the curves 2 and 3 calculated from (51) and (52), follows that there are significant quantitative and qualitative differences between the time (57) and phase (49), (50) averaging procedures. However, for the Sun's model ($\theta \ll 1$) with $h > 0$, the results of phase averaging (Fig. 12, curve 5) calculated according to the formula (53) approach asymptotically the results of time averaging (curve 4, obtained for $\theta_0 = 1$) with increasing external magnetic field. Such a difference between the phase and time averaging of Eq. (13) for the case of arbitrary θ and for the particular case of $\theta \ll 1$ are caused by the fact that the averaging procedures (49) and (50) consider incorrectly the weighting factors for the polar angle θ . One of the other evidence supporting this point is the expression for charge current I_c , determined on the base of (51) (or (52)) from the condition $\langle\partial U_0/\partial\tau\rangle = 0$,²⁰

$$I_c = \frac{2e}{\hbar\eta} a^2 l_m M_s H_k \quad (58)$$

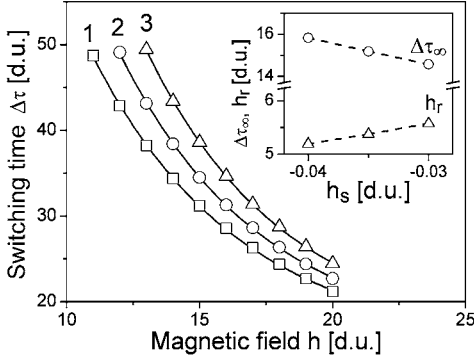


FIG. 15: Dependence of switching time $\Delta\tau$ on h for different spin currents: 1 - for $h_s = -0.030$, 2 - for $h_s = -0.035$, 3 - for $h_s = -0.040$. Behavior of the parameters $\Delta\tau_\infty$ and h_r with spin current h_s is given in the inset.

$$\times \frac{\alpha}{h} \left[h^2 + \frac{1}{4} \left(1 + \frac{h_p}{2} \right)^2 + \frac{5h_p^2}{32} \right],$$

which reveals an unexplainable divergence at $h \rightarrow 0$. At the same time, expression (54) practically corresponds to the averaging only over the angle φ , which – taking into account a good correlation of curves 4 and 5 (Fig. 12) – seems to be the most appropriate one. This result allows to simplify significantly initial equations (5), (6), and (13) by averaging their right-hand sides over φ . As a result, instead of (6) one obtains

$$\begin{aligned} \frac{\partial m_z}{\partial \tau} &= \alpha(1 + 0.5h_p)(1 - m_z^2)(m_z + \beta_p), \\ \frac{\partial \bar{\varphi}}{\partial \tau} &= -(1 + 0.5h_p)m_z + \alpha h_s - h. \end{aligned} \quad (59)$$

Instead of (5) and (13) it is possible to get correspondingly

$$\bar{U}_0 = (1 + 0.5h_p)(1 - m_z^2) - 2hm_z, \quad (60)$$

and

$$\frac{\partial \bar{U}_0}{\partial \tau} = -2\alpha(1 + 0.5h_p)^2(1 - m_z^2)(m_z + \beta_p)(m_z + \gamma), \quad (61)$$

with $m_z = \cos\theta$, $\beta_p \equiv (h + h_s/\alpha)/(1 + 0.5h_p)$ and $\gamma \equiv h/(1 + 0.5h_p)$.

The ordinary differential equations (59) are of separable-variable type and allow to find solutions for the averaged azimuthal angle $\bar{\varphi}$ at known $m_z(\tau)$ in the form

$$\varphi(\tau) = \bar{\varphi}(0) - (h - \alpha h_s)\tau - \left(1 + \frac{1}{2}h_p \right) \int_0^\tau m_z(\tau) d\tau, \quad (62)$$

where $\bar{\varphi}(0)$ is the initial value of the angle (i.e., its phase).

In the particular case of $\beta_p = \pm 1$, $m_z(\tau)$ can be found from the following transcendent equation:

$$\left[\operatorname{arctanh} m_z \mp \frac{1}{1 \pm m_z} \right] \quad (63)$$

$$- \left[\operatorname{arctanh} m_{z0} \mp \frac{1}{1 \pm m_{z0}} \right] = \mp 2\alpha(1 + 0.5h_p)\tau,$$

where m_{z0} is the initial value of the longitudinal magnetization vector component. As follows from Eq. (63), the sign change of the parameter β_p is equivalent to the simultaneous sign change of m_z and τ . It is worth noting, that despite the case $\beta_p = \pm 1$ was analyzed in detail²⁰ (see, for example, Eq. (19)) using numerical methods, the analytic equation for $m_z(\tau)$ was not presented there.

For $\beta_p \neq \pm 1$, $m_z(\tau)$ satisfies the following transcendent equation:

$$\begin{aligned} & \left(\frac{1 + m_z}{1 - m_z} \right)^{\beta_p} (1 - m_z^2)(m_z + \beta_p)^{-2} \\ &= \left(\frac{1 + m_{z0}}{1 - m_{z0}} \right)^{\beta_p} (1 - m_{z0}^2)(m_{z0} + \beta_p)^{-2} \\ & \times \exp[-2\alpha(1 + 0.5h_p)(1 - \beta_p^2)\tau]. \end{aligned} \quad (64)$$

It is easy to notice that expressions (62) and (64) are generalizations of formula (29) for the case of $h_p \neq 0$.

As the case $\beta_p = \pm 1$ (Eq. (63)) was already investigated in detail,²⁰ where it was used for determination of the threshold field $|h_{ac}^{(\pm)}|$ for the switching from parallel to antiparallel m_z state, we will consider below only the switching peculiarities defined by Eq. (64).

In Figs. 13 and 14 we present the time and field dependence of m_z and $\partial \bar{U}_0 / \partial \tau$, calculated according to Eqs. (64) and (61), respectively. The dashed areas in Fig. 13 correspond to $m_z(\tau)$ values obtained by the numerical integration of the system using the Runge-Kutta method. As one can see, for different values of h , $m_z(\tau)$ determined from Eq. (64) forms the outline of numerically calculated magnetization vector projection. It is worth noting that the good correlation between the analytical and numerical results can be also observed for the function $m_z(h)$ for different values of spin current h_s (Fig. 14). The latter proves that the proposed simplification of initial equations (5), (6), and (13) by averaging over φ is correct. The dashed curves in Figs. 13 and 14 correspond to time- and magnetic field-dependent values of $\partial U_0 / \partial \tau$, calculated on the base of Eqs. (61) and (64). Our analysis has shown that these curves can be approximated well with the Gaussian distribution.⁴¹ The values $m_{zm}(h, h_s, h_p, \alpha)$ corresponding to the minimum of $\partial U_0 / \partial \tau$, can be found by solving the cubic equation

$$m_{zm}^3 + \frac{3}{4}(\beta_p + \gamma)m_{zm}^2 + \frac{1}{2}(\gamma\beta_p - 1)m_{zm} - \frac{1}{4}(\beta_p + \gamma) = 0, \quad (65)$$

which can have one or three real solutions, of which only those satisfying the condition $-1 \leq m_{zm} \leq 1$ should be taken into account.

As follows from Fig. 13, at the fixed values of h_s , h_p and α , the minimum value of $\partial \bar{U}_0 / \partial \tau = f(h)$ decreases exponentially with time, while the similar minimum of $\partial \bar{U}_0 / \partial \tau = \psi(h_s)$ at fixed τ , h_p , and α grows linearly with

the increase of h_s (Fig. 14). It is important to emphasize that in the latter case the value of applied magnetic field, at which m_z turns to zero, decreases linearly with increasing h_s .

As one can see from Figs. 13 and 14, the switching time between the ground states $m_z = -1$ and $m_z = +1$ has the same order of magnitude as the half-width of the $\partial\bar{U}_0/\partial\tau$ peak. This half-width remains practically unchanged with h at the fixed τ , h_p , and α (Fig. 14), but depends significantly on the magnetic field with fixed h_s , h_p , and α (Fig. 13). As it turns out (Fig. 15), the half-width $\Delta\tau(h)$ of the peak $\partial U_0/\partial\tau = f(h, \tau)$ diminishes exponentially with increasing h according to formula

$$\Delta\tau = \Delta\tau_\infty + (\Delta\tau_0 - \Delta\tau_\infty)\exp(-h/h_r), \quad (66)$$

where the parameters $\Delta\tau_\infty$, $\Delta\tau_0$ and h_r depend on h_s , h_p , and α . It is worth noting that for the fixed applied magnetic field h , the increase of h_s leads to decrease of the switching time $\Delta\tau$. The dependence of the parameters $\Delta\tau_\infty$ and h_r on the spin current h_s are presented in the inset to Fig. 15. As one can see from this figure, $\Delta\tau_\infty$ and h_r are characterized by a linear decrease and increase with growing h_s , respectively. The results presented in Fig. 15 show that the increase of the absolute value of spin current leads to destabilization of the system, which now needs more time to switch between the ground states $m_z = -1$ and $m_z = +1$. To the contrary, the applied magnetic field has the stabilizing action, leading to a decrease of $\Delta\tau$. It is also worth to emphasize that for $h > 25$, the influence of the applied magnetic field becomes dominant compared to the role of the spin current h_s . It is worth noting that formulas (64) and (65) allow to obtain analytical expressions for the parameters (66), making it possible to investigate in detail the dependence of the switching time $\Delta\tau$ on h , h_s , h_p , and α .

IV. CONCLUSION

We have studied the magnetization dynamics of a ferromagnetic system subject to the spin-polarized current. We have used the methods of non-equilibrium thermody-

namics, which have been developed to describe the self-organization processes.^{34–37,50,51} Our results show that the ferromagnetic system displays a complex dynamics of instabilities with applied magnetic field and spin current. We have demonstrated that the method can be used to describe the dynamical properties of ferromagnetic nanostructures important for spintronics applications.

The behavior of equilibrium and stationary states has been investigated for a wide range of external parameters, without any limits on the angular variables describing the system magnetization. It has been shown that under certain conditions, the system can be switched to the oscillation mode regime with negligibly small damping. The phase portrait evolution has been investigated in detail for different values of external magnetic fields. The obtained results demonstrate a possibility to control the operating modes of the ferromagnetic components in spintronic devices by a proper choice of the ferromagnetic material with appropriate easy-plane anisotropy and the damping coefficient. It has been shown that the averaging of the initial system over the azimuthal angle allows to obtain analytical expressions, which make possible the detailed investigation of the switching peculiarities of the longitudinal magnetization between the states $m_z = -1$ and $m_z = +1$. The switching time has been analyzed in dependence on the external magnetic field and spin current.

The obtained results proves the successful application of self-organization methodology to solve theoretical problems of spintronics, which can yield new quantitative and qualitative results.

Acknowledgments

This work is partly supported by FCT Grant POCI/FIS/58746/2004 (Portugal) and the Polish State Committee for Scientific Research under Grants Nos. PBZ/KBN/044/P03/2001, 4 T11F 014 24 and 2 P03B 053 25. One of the authors (V.D.) thanks the Calouste Gulbenkian Foundation in Portugal for support.

[†] E-mail: horley@cv.ukrtel.net

¹ I. Žutic, J. Fabian, and S. Das Sarma, Rev. Mod. Phys. **76**, 323 (2004).

² D. K. Young, J. A. Gupta, E. Johnston-Halperin, R. Epstein, Y. Kato, and D. D. Awschalom, Semicond. Sci. Technol. **17**, 275 (2002).

³ G. Schmidt and L. W. Molenkamp, Semicond. Sci. Technol. **17**, 310 (2002).

⁴ S. J. Pearton, C. R. Abernathy, D. P. Norton, A. F. Hebard, Y. D. Park, L. A. Boatner, J. D. Budai, Mater. Sci. Eng. **R40**, 137 (2003).

⁵ T. Dietl, Semicond. Sci. Technol. **17**, 377 (2002).

⁶ D. Ferrand, A. Wasiela, S. Tatarenko, J. Cibert, G. Richter, P. Grabs, G. Schmidt, L. W. Molenkamp, and T. Dietl, Sol. State Commun. **119**, 237 (2001).

⁷ S. Das Sarma, J. Fabian, X. Hu, and I. Žutic, Sol. State Commun. **119**, 207 (2002).

⁸ D. Grundler, Phys. Rev. B **63**, 161307(R) (2001).

⁹ I. Žutic, J. Fabian, and S. Das Sarma, Appl. Phys. Lett. **79**, 1558 (2001).

¹⁰ J. Barnaś and A. Fert, Phys. Rev. Lett. **80**, 1058 (1998).

¹¹ J. A. Katine, F. J. Albert, R. A. Buhrman, E. B. Myers, and D. C. Ralph, Phys. Rev. Lett. **84**, 3149 (2000).

¹² V. K. Dugaev, Yu. Vygranenko, M. Viera, V. I. Litvinov, and J. Barnaś, Physica E (Amsterdam) **16**, 558 (2003).

- ¹³ M. I. D'yakonov and V. I. Perel', Phys. Lett. A **35**, 459 (1971).
- ¹⁴ M. I. D'yakonov and V.I. Perel', Pis'ma Zh. Eksp. Teor. Fiz. **13**, 206 (1971) [JETP Lett. **13**, 144 (1971)].
- ¹⁵ M. I. D'yakonov and V. I. Perel', Pis'ma Zh. Eksp. Teor. Fiz. **13**, 657 (1971) [JETP Lett. **13**, 467 (1971)].
- ¹⁶ E. I. Rashba, Phys. Rev. B **62**, R16267 (2000).
- ¹⁷ E. I. Rashba, Eur. Phys. J. B **29**, 513 (2002).
- ¹⁸ J. C. Slonczewski, J. Magn. Magn. Mater. **195**, L261 (1999).
- ¹⁹ J. C. Slonczewski, J. Magn. Magn. Mater. **159**, L1 (1996).
- ²⁰ J. Z. Sun, Phys. Rev. B **62**, 570 (2000).
- ²¹ Z. Li and S. Zhang, Phys. Rev. B **68**, 024404 (2003).
- ²² Z. Li and S. Zhang, Phys. Rev. Lett. **92**, 207203 (2004).
- ²³ Z. D. Li, J. Q. Liang, L. Li, and W. M. Liu, Phys. Rev. E **69**, 066611 (2004).
- ²⁴ Z. Li and S. Zhang, Phys. Rev. B **69**, 134416 (2004).
- ²⁵ S. Urazhdin, Phys. Rev. B **69**, 134430 (2004).
- ²⁶ J. Fernández-Rossier, M. Braun, A. S. Núñez, and A. H. MacDonald, Phys. Rev. B **69**, 174412 (2004).
- ²⁷ M. D. Stiles and A. Zangwill, J. Appl. Phys. **91**, 6812 (2002).
- ²⁸ M. D. Stiles and A. Zangwill, Phys. Rev. B **66**, 014407 (2002).
- ²⁹ M. D. Stiles, J. Xiao, and A. Zangwill, Phys. Rev. B **69**, 054408 (2004).
- ³⁰ Ya. B. Bazaliy, B. A. Jones, and S. C. Zhang, Phys. Rev. B **69**, 094421 (2004).
- ³¹ M. d'Aquino, C. Serpico, G. Miano, I.D. Mayergoyz, and G. Bertotti, J. Appl. Phys. **97**, 10E319 (2005).
- ³² I. Mayergoyz, M. Dimian, G. Bertotti, and C. Serpico, J. Appl. Phys. **97**, 10E0509 (2005).
- ³³ G. Bertotti, C. Serpico, I.D. Mayergoyz, A. Magni, M. d'Aquino, and R. Bonin, Phys. Rev. Lett. **94**, 127206 (2005).
- ³⁴ G. Nicolis and I. Prigogine, *Self-Organization in Nonequilibrium Systems* (Wiley, New York, 1977).
- ³⁵ H. Haken, *Advanced Synergetics* (Springer, Berlin, 1983).
- ³⁶ W. Ebeling, *Strukturbildung bei Irreversiblen Prozessen* (Teubner, Leipzig, 1976).
- ³⁷ Yu. L. Ermolaev and A. L. Sanin, *Elektronnaya Sinergetika* (in Russian) (Leningrad Univ. Publ., Leningrad, 1989).
- ³⁸ L. D. Landau and E. M. Lifshitz, Phys. Zh. Sowjetunion **8**, 153 (1935).
- ³⁹ K. P. Belov, A. K. Zvezdin, A. M. Kadomtseva, and R. Z. Levitin, *Orientation Transitions in Rare-Earth Magnetics* (Nauka, Moscow, 1979).
- ⁴⁰ L. D. Landau and E. M. Lifshitz, *Statistical Physics* (Pergamon, Oxford, 1980).
- ⁴¹ M. Abramowitz and I.A. Stegun (Eds.), *Handbook of Mathematical Functions* (National Bureau of Standards, Applied Mathematics Series **55**, 1964).
- ⁴² S. V. Vonsovskii, *Magnetism* (Wiley, New York, 1974).
- ⁴³ N. P. Erugin, I. Z. Shtokalo et al. *Ordinary Differential Equations* (Vyshcha Shkola, Kiev, 1974).
- ⁴⁴ Zh. Yoss and D. Joseph, *Elementary Stability and Bifurcation Theory* (Mir, Moscow, 1989).
- ⁴⁵ L. A. Ostrovskiy, *General Theory of Electronic Measuring Devices* (Energiya, Leningrad, 1971).
- ⁴⁶ J.A. Sanders, F. Verhulst, *Averaging Methods in Nonlinear Dynamical Systems* (Springer Verlag, New York, 1985).
- ⁴⁷ A. H. Nayfeh, *Introduction to Perturbation Techniques* (Wiley, New York, 1993).
- ⁴⁸ L. I. Sedov, *Similarity and Dimension Methods in Mechanics* (CRC Press, Boca Raton, 1993).
- ⁴⁹ E. Kamke, *Ordinary Differential Equations Handbook* (Mir, Moscow, 1984).
- ⁵⁰ P. N. Gorley, P. P. Horley, and P. M. Tomchuk, Techn. Phys. Lett. **25**, 7 (1999) [Pis'ma v ZhTF **25**, 17 (1999)].
- ⁵¹ P. P. Horley, *Dynamic Chaos and Self-Organization in Bipolar Semiconductors with Drift Instability*, Ph.D. Thesis, Chernivtsi, 1999.